Changes in extreme wave events in the southwestern South Atlantic Ocean

Carolina B. Gramcianinov[1] · Joanna Staneva[1] · Ricardo de Camargo[2] · Pedro L. da Silva Dias[2]

Abstract

The southwestern South Atlantic (SWSA) has faced several extreme events that caused coastal and ocean hazards associated with high waves. This study aimed to investigate the extreme wave climate trends in the SWSA using percentile- and storm-based approaches to determine potential coastal impacts. Changes in extreme wave event characteristics were evaluated through distribution maps and directional density distributions. Our results showed an overall increase in the 95th-percentile of the significant wave height (Hs), mostly in the northern and southern portions of the domain. There was a general increase in the area affected by the events and in their lifetimes in the austral summer. In contrast, winter events had higher maximum intensities, which were not homogeneous throughout the domain. Changes in the wave power direction affected most of the analysed locations, showing a clockwise shift of summer events and a large directional spread of events from the southern quadrant (SW–SE). These changes were related to the southwards shift of the subtropical branch of the storm track, reflecting increased cyclonic activity at 30° S (summer) and 45° S (winter). These storm track shifts allowed the development of large fetches on the southern edge of the domain, promoting the propagation of long waves.

Keywords Coastal hazards · Wave climate · South America · Extratropical cyclones · Storm track

1 Introduction

In recent years, the South Atlantic Ocean has faced several extreme events related to changes in climate patterns (Mar-

✉ Carolina B. Gramcianinov
  carolina.gramcianinov@hereon.de

  Joanna Staneva
  joanna.staneva@hereon.de

  Ricardo de Camargo
  ricado.camargo@iag.usp.br

  Pedro L. da Silva Dias
  pedro.dias@iag.usp.br

[1] Institute for Coastal Systems Analysis and Modeling, Helmholtz-Zentrum Hereon, Max-Planck-Straße 1, Geesthacht 21502, Germany

[2] Institute of Astronomy, Geophysics and Atmospheric Science, University of São Paulo, Rua do Matão, 1226, São Paulo 05508-090, Brazil

cello et al. 2018; Rodrigues et al. 2019; Dalagnol et al. 2022). These changes have been reflected in hazards in the southwestern South Atlantic (SWSA; Fig. 1) associated with wind and waves, such as extreme waves and storm surges (e.g., Souza et al., 2019). With its strategic location, the SWSA region has high oil and gas production demands and hosts the most economically important harbours in South America, through which 755 million tons of goods were transported in 2021 ANTAQ (2022). In addition, the coastal population between 15° S and 40° S contains approximately 20 million people who are highly vulnerable to coastal erosion and coastal infrastructure damage (Zamboni and Nicolodi 2008). The SWSA coastal regions hold rich biodiversity as they contain a portion of the Brazilian coastline; Brazil has more than 7400 km of coastline, an exclusive economic zone of 3.6 million km^2, and 9.4% of the mangroves growing globally (U.N. 1982; Hamilton and Casey 2016). The south and southeastern Brazilian coasts, directly embedded in the SWSA, contain important ecosystems, including coral reefs and 856 km^2 of mangroves; thus, these regions are crucial for the economic activities and cultural identity of the area (Pereira-Filho et al. 2021; ICMBio 2018). However, the coastal and oceanic structures, as well as the local operations, are usually designed

based on MetOcean statistics that do not correctly address climatic shifts (e.g., Takbash and Young, 2020).

The wave climate in the SWSA is mainly controlled by the storm track and South Atlantic Subtropical High (SASH). The former is associated with the most extreme events due to the strongest winds associated with extratropical cyclones (e.g., da Rocha et al. 2004; Campos et al. 2018). This storminess exhibits distinct seasonal characteristics, with the storm track shifting northwards during the winter and more severely affecting the SWSA. However, during summer, some storms develop along the Brazilian coast in the region of approximately 30° S (Hoskins and Hodges 2005; Reboita et al. 2010). The proximity of this region to the coast increases the potential danger associated with these storms, even with their low-frequency occurrence, mainly due to the inherent difficulties associated with predicting storm locations and intensities.

Several limitations hinder the study of mean and extreme wave climate and trends in the South Atlantic. Some of the problems with these existing methods are widely known: the internal variabilities in model systems are sometimes higher than the corresponding change signals; the lack of long-term temporal observation data hampers satellite and model product validation and calibration; and, consequently, the hindcast and forecast quality of existing models are hindered. Other problems associated with the study region are the still-limited knowledge and understanding of the local physical processes and climate variabilities. The limited accuracy of long-term integrations and the scarce data availability can compromise these analyses. Predicting waves in the SWSA region is challenging because this area generally presents a hybrid sea state with superpositioned swells and wind-sea waves.

Some recent studies have revealed changes in the wave pattern in the South Atlantic, although they usually focused on global rather than regional features. Young and Ribal (2019) examined the trends in global wind speed and significant wave height (Hs) distributions. While the wind distribution was broadening, along with increases in the mean, mode, and percentile values, the Hs distribution was reportedly skewing to the left towards an increased frequency of small waves. The Southern Ocean (SO), in turn, appeared as an outstanding region, experiencing an increase in the extreme waves, as indicated by satellite data (the 90th-percentile waves, Young and Ribal 2019) and reanalysis products (centennial Hs values, Takbash and Young 2020). In general, most previous studies have reported increases in wave height extremes in the Southern Hemisphere (SH) over the past 41 years. This increase is expected to continue in the future (Caires and Sterl 2005; Dobrynin et al. 2012; Lemos et al. 2019).

In addition to understanding the significant wave height trends, it is important to assess changes in wave event characteristics, such as the mean wave direction, peak period,
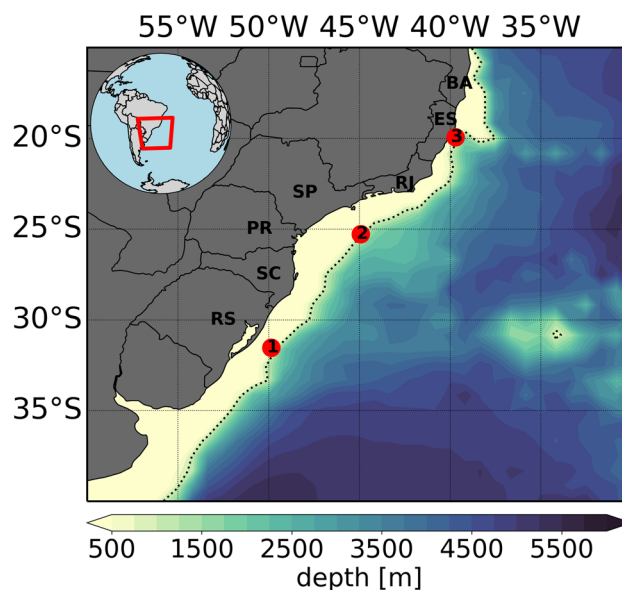

Fig. 1 Study domain with bathymetry (ETOPO1; Amante and Eakins 2009). The Coastal Brazilian states are marked as follows: RS, Rio Grande do Sul; SC, Santa Catarina; PR, Paraná; SP, São Paulo; RJ, Rio de Janeiro; ES, Espíto Santo; and BA, Bahia. The location of the three buoys used in this work is marked with red dots: (1) Rio Grande (RG), (2) Santos (SP), and (3) Vitória (ES)

and wave power. Some previous works reported an increase in the wave power over the South Atlantic under the present climate conditions (Reguero et al. 2019; Odériz et al. 2021). The trends reported by Odériz et al. (2021) exist for the waves generated by the easterlies and westerlies in the subtropics and extratropics, respectively. Changes related to waves in the Atlantic are not restricted to the wave power but include a general shift in the mean wave direction (Hemer et al. 2010) and an increase in the peak period (Lobeto et al. 2021). In fact, Lobeto et al. (2021), using directional wave spectra produced by present and future climate simulations, found that the peak period of the easterly waves is projected to decrease while it is projected to increase in the south/southeasterly waves. Nevertheless, the South Atlantic has not been deeply explored in global studies due to its weak signal compared to other ocean bases, such as the North Atlantic. However, the wave climate variations suggested by the studies mentioned above may act directly on the Brazilian coastline, as reported by Silva et al. (2020). These authors, using historical shoreline records and wave modelling, showed how the oscillation between the south and east dominant wave energy fluxes has led to changes in the coastal morphodynamics at both the regional and local scales.

With this in mind, we aim to investigate the extreme wave climate trends in the SWSA while focusing on the changes in the wave event characteristics and their potential effects on the Brazilian coast and continental shelf. Thus, we examine the long-term average statistics and climatic trends

between 1979 and 2020 using a set of wave products derived from models and satellites. At first, both traditional (i.e., percentile-based) and event-based approaches are used to provide an overview and new insights into the regional wave climate and the observed changes. Second, a detailed analysis of the directional wave power and peak period changes is performed to explore further the extreme event changes, their drivers, and their potential impact on the coastal area. In the analyses, we consider the entire annual period but focus on changes in the summer and winter seasons. The outcomes of this work contribute not only to the extreme wave climate knowledge in the study region but also to the discussion on how large-scale changes impact the coastal and offshore regions of the SWSA. Understanding the effect of the present changes in this region is still not well documented and is crucial for future offshore and coastal structure and activity management.

2 Data and methods

2.1 Datasets

The main dataset used in this work is ERA5 (Hersbach et al. 2020), the 5th generation of reanalysis product released by the ECMWF. We use the 1-hourly ERA5 products from 1979 to 2020 provided by the Copernicus Climate Center Service (C3S 2017) available at 0.25° and 0.5° of horizontal resolutions for the atmospheric and wave parameters, respectively. Several studies have shown the advantages associated with using ERA5 compared to its predecessor (e.g., Belmonte Rivas and Stoffelen 2019; Hersbach et al. 2020). ERA5 wave products present good performances even in coastal areas when evaluated against in situ measurements (buoys), as shown in Supplementary Text .

To evaluate the ERA5 percentile trends, we used the Australian Ocean Data Network (AODN) satellite products, specifically a multiplatform cross-calibrated dataset (Young and Ribal 2019). The AODN collects measurements from 13 altimeters and cross-calibrations using altimeters, radiometers, scatterometers, and the National Data Buoy Center (NDBC) buoys (Young and Ribal 2019). The AODN altimeter database is built using 13 satellites: CRYOSAT2, ENVISAT, ERS1, ERS2, GEOSAT, GFO, HY2, JASON1, JASON2, JASON3, SARAL, SENTINEL3A, and TOPEX. It is available in 1° x 1° bin files covering the timespan from 1985 to the present day. However, for the ERA5 evaluation conducted herein, we consider the period from 1993 to 2019, thus allowing the inclusion of the data that is cross-validated (Young and Ribal 2019). ERA5 assimilates the Hs from 6 of these satellites: CRYOSAT2, ENVISAT, ERS1, ERS2, JASON1, and SARAL. However, the postprocessing of the data assimilated by ERA5 is distinct from the AODN dataset,

resulting in different outcomes, especially under extreme wave conditions (Campos et al. 2022).

We also compare the derived percentiles with those of five more wave products: the University of Melbourne's global wave hindcasts (UMelb) (Liu et al. 2021); the Copernicus Marine Service global hindcast (CMEMS) (Law-Chune et al. 2021); and both of the Ifremer hindcasts forced with ERA5 and Climate Forecast System Reanalysis (CFSR, Saha et al. 2010) winds (Rascle and Ardhuin 2013), defined hereafter as Ifremer-ERA5 and Ifremer-CFSR, respectively. The CMEMS hindcast is available at a 0.20° horizontal grid from 1993 to 2020. The wave field is produced by Meteo France Wave Model version 4 (MFWAM v4 with ST4), which is forced by surface winds and the sea ice fraction derived from ERA5 and ocean currents obtained from the ocean reanalysis Global Ocean Reanalysis and Simulation (GLORYS). The UMelb wave products are available from 1980 to 2019 at a 0.25° horizontal grid. This hindcast is produced using wave model WAVEWATCH III (WW3; WW3 Development Group, 2019) with the state-of-the-art source term ST6, which is based on observations (Liu et al. 2019), and is forced by ERA5 10-m winds and satellite-derived sea ice concentrations. The Ifremer hindcasts are available at a 0.5° horizontal grid covering the period between 1992 and 2019. They are produced through WW3 with ST4 (Ardhuin et al. 2010). Both versions are forced by CFSR sea ice and have no current forcing.

It is important to note that it is difficult to evaluate the performance of the ERA5 product before the 1990s in the SWSA, as satellite and buoy data from this time are rare and/or inconsistent. The ERA5 performance may be compromised due to the lack of data available for assimilation during this early period. A brief discussion on this matter can be found in Supplementary Text . Even considering these limitations, we believe that it is important to access the long-term reanalysis product to create a reference for changes that the scientific community and society can use.

2.2 Percentile computation

In this study, percentiles are determined based on the empirical distribution of Hs values within a specific time period. Various methods are employed to select the appropriate Hs value depending on the dataset (see Table 1). The percentiles are computed for grid points within the domain considering the time series of Hs. The empirical distribution is built based on the Hs peaks within 48 h. This time window allows us to obtain a more detailed view of individual wave event occurrences, assuring that only one peak per storm is used to construct the Hs distribution (e.g., Caires and Sterl 2005; Meucci et al. 2020). The exception is for the satellite data, which has Hs measurements approximately every 7 days. The subsampling of storms from satellite data affects the

Table 1 Information about the methods used for the percentile computation in each dataset and analysis

Dataset	Analysis	Computed percentile	Method to compute the perc. at each grid point	Percentile output	Method to plot
ERA5	Weisse and Günther (2007)	95th	Hs peak in 48 h	2D, 1 for each season	—
Satellite data	Percentile trend	95th	Sampled Hs (each 7 days)	2D, monthly	Spacially averaged and maximum perc. per season
ERA5 + hindcasts	Percentile trend	95th	Hs peak in 48 h	2D, monthly	Spacially averaged and maximum perc. per season
ERA5 + buoy	Directional analysis	75th and 95th	Hs peak in 48 h	1 for each season	—

percentile computations, and this is a limitation concerning the use of satellite products for storm wave analyses. Nevertheless, we prefer to keep this data in the analysis, using the sampled Hs to obtain the percentile rather than relying on the Hs peaks. The results of this percentile computation are monthly percentile spatial distributions for each dataset used to compute the spatial trends. To compare the trends among the datasets, these monthly percentile fields were spatially averaged, and the maximum percentile per season was used. We choose to use the maximum monthly percentile in a given season as its value are close to the seasonal percentile (obtained using the Hs peaks within the 3 months; Suppl. Material Fig. S1). We focus our analysis on the summer and winter, which are defined respectively as December-January-February (DJF) and June-July-August (JJA). The summer of a year includes December of the last year (e.g., the summer of 2020, consider December from 2019). In this way, the first year (1979) is not considered in the summer analysis since data from 1978 are not available.

A similar approach was used to obtain the threshold used to select extreme events when applying the Weisse and Günther (2007) method (Sect. 2.3) and directional analysis (Sect. 2.4). However, in those cases, the empirical distribution was built by collecting the Hs peaks in a time series

composed of the months in a selected season from the whole available period. These computations result in one percentile field per season for the whole period, as seen in Fig. 2.

2.3 Wave event analysis

The wave event statistics are derived following the methods developed by Weisse and Günther (2007), in which consecutive points over a specific threshold within a given time series are considered to define extreme wave events. This event-counting process is performed for each grid cell considering its unique severe event threshold (SET), defined herein as the 95th-percentile of the ERA5 Hs value computed for the whole period (1979–2020). Notably, there is no widely accepted method for selecting threshold values, and Hs values between the 90th and 99th-percentile are often used (e.g., Leo et al. 2020; Campos et al. 2019). In general, a high threshold is a valid choice when the data sample is sufficiently large and when the focus is on the most extreme events. The duration of each event is computed by counting the number of time steps during which the curve is above the SET value. The intensity is equal to the difference between the maximum Hs of the event and the SET. Other parameters can also be added to each event to build a set of statistical

Fig. 2 Spatial distribution of the 95th-percentile Hs (m) in **a** summer (DJF) and **b** winter (JJA) for the ERA5 product spanning the period from 1979 to 2020
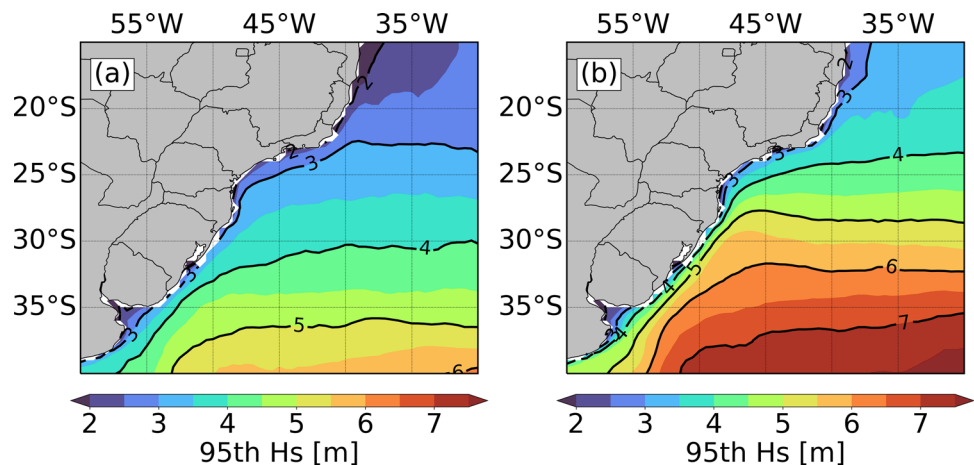
products, such as the peak period and mean wave direction. In this case, the peak period and mean wave direction representative of an event are computed by the average of all time steps of the event. The wave event statistics are presented as spatial distributions corresponding to each parameter. It is important to note that, in our seasonal analyses, we used a seasonal threshold, i.e., the 95th-percentile computed for the months within each season. This approach respects the distribution of each season, particularly when they present different wave sources (Goda 2010).

2.4 Directional density distributions

Directional density distributions were computed for both the wave power and peak period. We compute the wave power or wave energy flux following Eq. 1 (Guillou 2020):

$$P = (\frac{\rho \, g^2}{64 \, \pi}) \, Hs^2 \, Te, \tag{1}$$

where P is the wave energy flux per unit of wave crest length (W/m), ρ is the water density, g is the acceleration due to gravity, Hs is the significant wave height, and Te is the wave energy period. Te was estimated based on its relation with the peak period (Tp), which depends on the wave spectrum shape defining the sea state (Cornett 2008). Considering that the SWSA is subjected to a standard JONSWAP spectrum, we can assume a conservative approximation that $Te = 0.9 \times Tp$ (Guillou 2020). This approximation is used in several studies, both in global (e.g., Cornett 2008) and regional (e.g., Wu et al. 2015; Guillou 2020) approaches.

We compute the directional distributions using only segments of the wave parameter time series when $Hs > Hs_{p75}$, where Hs_{p75} is relative to the Hs records at that point and computed using Hs peaks as described in Sect. 2.2. Although the 75th-percentile is not formally considered an extreme threshold, it allows the consideration of more events with medium to high severity and follows the same behaviour of the distribution obtained using the Hs_{p95} (Suppl. Text 1, Figs. S8 to S13). Due to the greater number of events retained with the Hs_{p75}, the statistic becomes more robust and can be useful to the assessment of severe events, which are relevant, particularly due to the proximity of the analysed points to the coast. The density distribution of the parameters against the directions was computed using a Gaussian kernel density estimation (KDE), which is a non-parametric method to estimate the probability density function of a variable. Using density instead of a simple histogram (i.e., a wave rose) improves the visualisation of the trends against the 42-year climatology. The wave parameters extracted from the time series were used to build a KDE, which then estimates their probabilistic density function in a regular grid

with 33×33, which means having 33 increments for both directions (angles) and variable units (wave power or period). This new grid is plotted in polar projection, based on the angles (directions, from) from 0 to 2π ($\Delta_\theta = 11.25°$) and radius from 0 to 150 ($\Delta_r = 4.7 \, kWm^{-1}$) for the wave power and from 0 to 20 ($\Delta_r = 0.625 \, s^{-1}$) for the peak period.

2.5 Cyclone diagnostics

The cyclone track information used to build cyclone centre density maps was obtained from the "Atlantic extratropical cyclone tracks database" provided by Gramcianinov et al. (2020), which covers the entire Atlantic Ocean over the period from 1979 to 2020. Cyclones are tracked based on ERA5 fields (winds at 850 hPa) using the TRACK algorithm (Hodges 1994, 1995), following the minimum duration and displacement requirements of 24 h and 1000 km, respectively. More information regarding the method and database evaluation is available in Gramcianinov et al. (2020).

The density analysis is also conducted using the KDE method (Hodges 1996) using the central point of the cyclones during all time steps of their lifetime, i.e., not considering a specific or unique time step along the track as made by Hoskins and Hodges (2002). In this way, it is possible to assess the persistence of a given cyclone within a region. The same method is applied with the location (latitude and longitude) of the maximum wind speed at 10 m within a 6° radius from the cyclone centre; this value is typically used as an intensity measurement (Hodges et al. 2011) and is used herein as an indication of the fetch position.

2.6 Trends estimation and testing

Trends were estimated based on Sen's slope estimator (Sen 1968), which evaluates the magnitude of a time series trend. The significance of Sen's slope was calculated by the Mann-Kendall test (Mann 1945; Kendall 1975). During the analysis, we considered a p-value lower than 0.05 as a metric for significance. However, as this fixed threshold can be subjective, the p-values are also presented (Suppl. Material, Figs. S4, and S5). Both methods are non-parametric (distribution-free) procedures and consider the monotonic upward or downward of the time series, thus being more robust to climate-based analysis (e.g., Wang et al. 2020).

3 Results

3.1 Overview of extreme wave climate

The SWSA extreme wave climate is mainly controlled by the propagation of low-pressure transients between 55° S and 30° S, characterising the distribution of the intensity of

extreme wave events by a gradient towards the south in both seasons (Fig. 3b, e). The influence of the storm track in the regional wave climate reflects the dominant southerly waves (Fig. 3d, h).

In summer, the main storm track shifts polewards, limiting high waves to the southern portion of the study domain. Nevertheless, extreme wave events are mostly experienced along the Brazilian coast up to 15° S, despite their low intensity (Fig 3a, b). The northern part of the domain, where the number of extremes is higher (Fig. 3a), is locally dominated by the easterlies from the SASH circulation and post frontal anticyclone in the summer (Fig. 3c). The central and southern portions are more influenced by subtropical storms and northwest/southeast-oriented quasi-stationary fronts that support the formation of the South Atlantic convergence zone (SACZ) (Kodama 1992; Pezzi et al. 2022). In this way, summer events are forced mainly by local atmospheric systems, resulting in a longer lifetime (Fig. 3c, g) and a lower peak period (see Supp. Material, Fig. S2) than winter events.

The winter, in turn, presents a more homogeneous distribution of extreme events in the region. Thus, all points are equally likely to surpass the 95th-percentile Hs threshold. The cold season has a higher number of extreme wave events and the most intense ones (e.g., Machado et al. 2010; Gramcianinov et al. 2020). The whole study domain is dominated by extreme southerly waves (Fig. 3h) due to the northwards shift of the main storm track (Hoskins and Hodges 2005). Typically, in winter, the SWSA presents relatively long fetches along the coast (southwest/northeast orientated) associated with cyclones generated at approximately 35° S (Gramcianinov et al. 2020). Rear anticyclones can widely intensify these fetches on the western side of the extratropical cyclone, developing a pattern that is widely related to the most severe cases observed in the domain (e.g., da Rocha et al. 2004; Machado et al. 2010; Dragani et al. 2013). The influence of these extratropical systems allows the development of highly energetic waves with long periods (Suppl. Material, Fig. S2). However, the winter events have shorter lifetimes than the summer events (Fig. 3g), as the extratropical cyclones move faster in the winter (Gramcianinov et al. 2020).

3.2 Change in 95th-percentile Hs

First, we present the 95th-percentile Hs (Hs_{p95}) trends to discuss the general behaviour of this important extreme wave parameter, as well as to evaluate the use of the ERA5's long time series available to the present study. The datasets used in this comparison are the UMelb, CMEMS, Ifremer-ERA5, Ifremer-CFSR, and AODN satellite data.

Considering the domain-averaged value of the maximum monthly Hs_{p95} in a given season, the only season with a significant trend is the summer (Fig. 4a) for the two long-time

series, ERA5, and UMelb, with 0.75 and 0.57 cm/year, respectively (Mann-Kendall test; p-value $\leq$ 0.05). Time series that start in 1993, including the one derived from the satellite data, present no significant positive trend (high p-value). In fact, neither ERA5 nor UMelb presents significant trends for the summer when considering the short period between 1993 and 2019 (Suppl. Material, Figs. S3). However, we can see agreement among the datasets regarding their behaviour around the peaks and valleys of the time series.

The Hs_{p95} trends signal for the winter (Fig. 4c) presents more disagreement among the datasets. Despite a fair accordance of seasonal peaks, their magnitude varies. No trends are statistically significant in this season.

The wide range of Hs_{p95} trends is due to differences in the period, forcing, and models, as reported by previous studies (Sharmar et al. 2021; Casas-Prat et al. 2022). The disagreement among the datasets is prominent in the winter values, while there is a certain level of consistency in the trend signal in the summer data.

The lack of agreement between the datasets regarding the trend obtained by the domain-averaged Hs_{p95} can also be justified by the spatial heterogeneity of the field (Fig. 4b, d). The winter spatial Hs_{p95} trends reveal positive values in the southern and northern portions of the domain, while the centre presents negative values (Fig. 4d). Statistically significant trends (p-value $\leq$ 0.05) are present at only approximately 35.75° S/35° W ($\sim$ 3 cm/year) and 15° S/32° W in the winter ($\sim$ 2 cm/year). Summer, in turn, presents positive trends in most of the study region, with significant values ranging from 1 to 2.5 cm/year (Fig. 4b). The southern and northern portions have higher trends, while the central portion presents a lack of significant trends.

3.3 Extreme wave events changes

Spatial differences between the datasets covering different periods are expected and can smooth long-term changes. This section and the following sections explore changes in the extreme wave event parameters based on the more extended dataset, ERA5 (42 years), which presents good agreement with buoy data offshore of the Brazilian coast (Suppl. Text 1). Despite the issue regarding the homogeneity of modern reanalysis (Casas-Prat et al. 2022), we consider ERA5 a powerful and widely used tool to assess trends in the South Atlantic. To support significant trends discussion, the p-value spatial distribution for each field is available in the Suppl. Material (Figs. S4 and S5).

The extreme wave events averaged over the study domain (Fig. 4) show that the area affected by extreme events ($0.37 \times 10^6 km^2$/year) and the lifetime of the events (0.14 h/year) increase in summer. On the other hand, a significant increase in the maximum intensity of extreme events (1.5 cm/year)
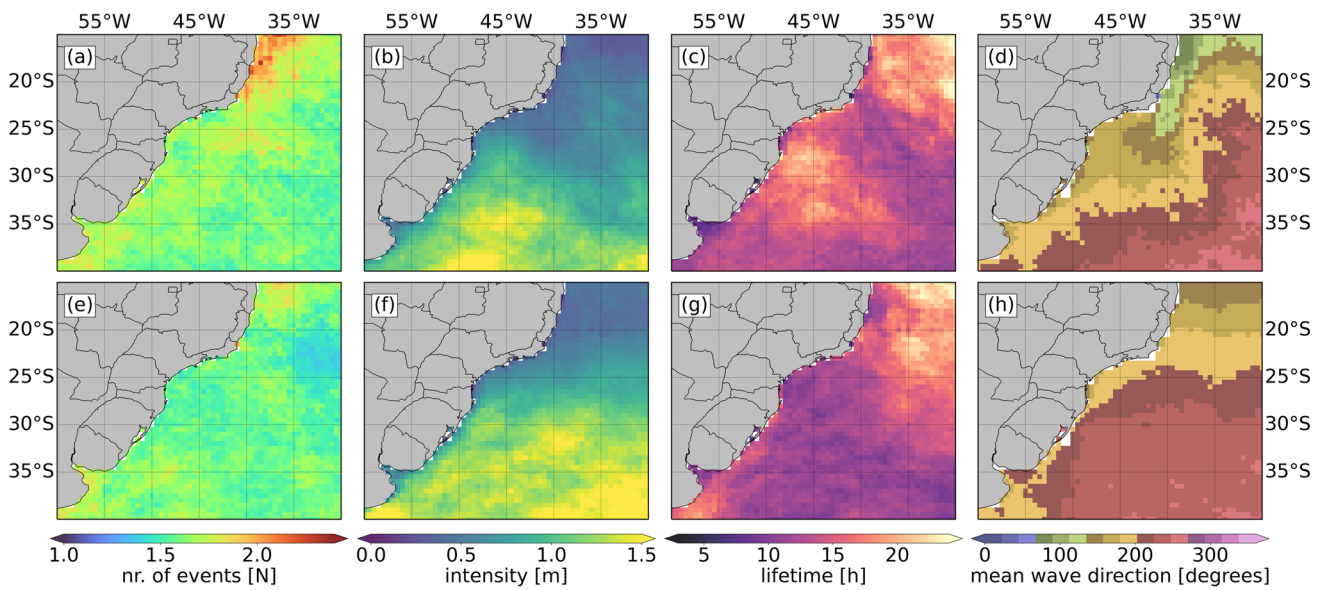
Fig. 3 **a** and **e** Mean number of storm wave events per grid point per season, **b** and **f** mean intensity (Hs$_{peak}$ - 95th Hs), **c** and **g** mean lifetime, and **d** and **h** mean wave direction of the events in the **a–d** summer (DJF) and **e–h** winter (JJA). The mean wave direction is oriented as 0° and 90° equal to North and East, respectively.

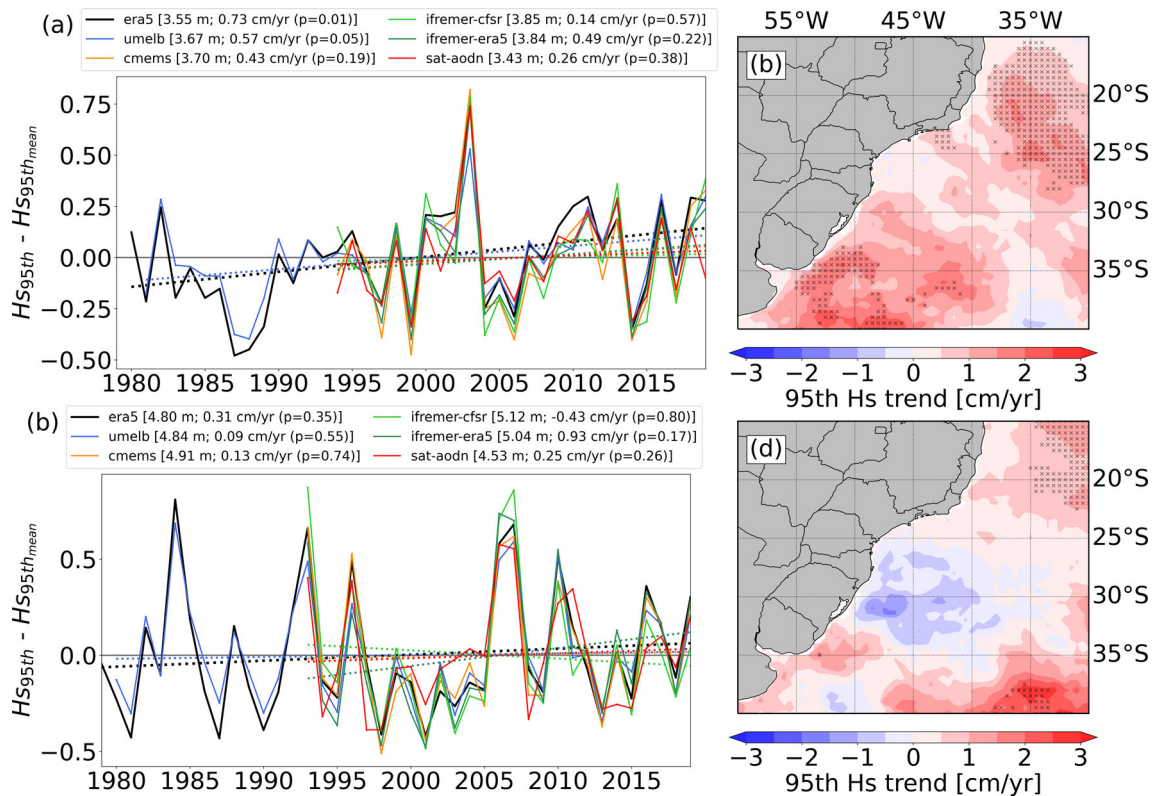The analysis was obtained from the ERA5 product spanning the period from 1979 to 2020

Fig. 4 Temporal evolution of the domain-averaged value of the maximum monthly Hs$_{p95}$ in the **a** summer (DJF) and **c** winter (JJA) (minus the time series mean) in the ERA5, UMelb, CMEMS, Ifremer-CFSR, Ifremer-ERA5, and AODN satellite products. Legends indicate the mean, trend, and p-value based on the Mann-Kendall test. Spatial distri-

bution of temporal trends was derived for **b** summer (DJF) and **d** winter (JJA). The grey crosses indicate trends with p-value ≤ 0.05 (Mann-Kendall test), and the p-values spatial distributions are presented on Suppl. Material Fig. S4
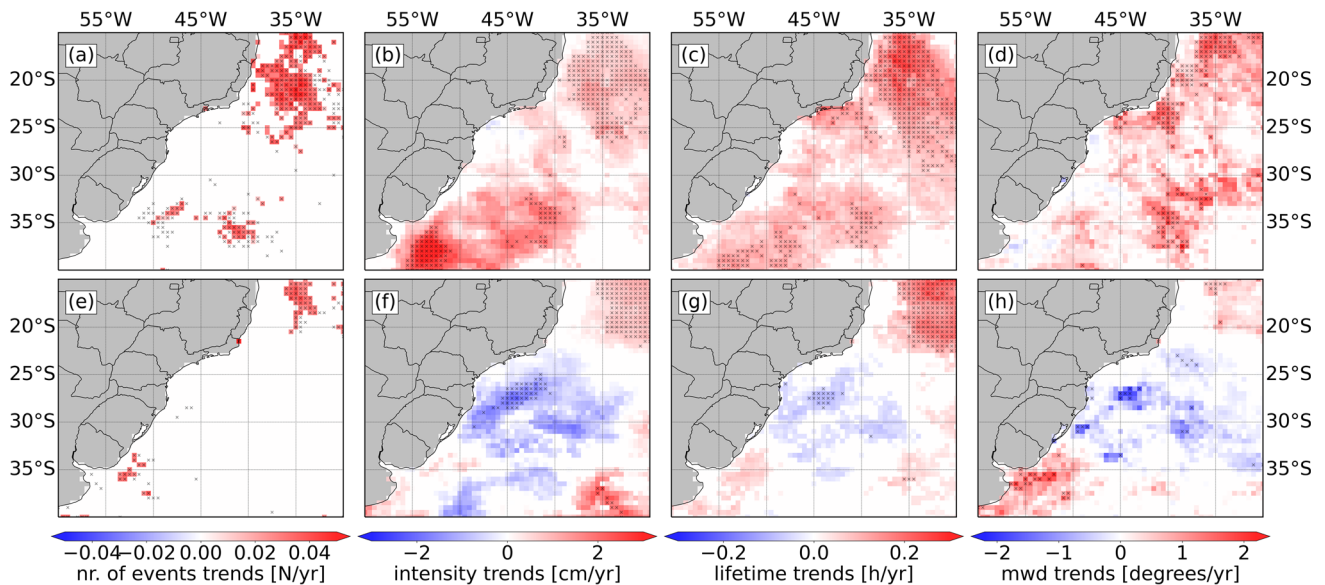
Fig. 5 **a** and **e** Trends of the seasonal number of events, **b** and **f** maximum intensity (Hs - 95th-percentile Hs), **c** and **g** mean lifetime (hours), and **d** and **h** mean wave direction of events (degrees) in the **a**–**d** summer (DJF) and **e**–**h** winter (JJA). The grey crosses indicate p-value ≤ 0.05 (Mann-Kendall test), and the p-values spatial distributions are presented on Suppl. Material Fig. S5

occurs in winter. All these trends present a p-value < 0.05 (Mann-Kendall test).

The spatial changes in the characteristics of the events resemble the percentile patterns (Fig. 4b, d), with significant positive trends found for the lifetime (0.1–0.3 h/year) and mean intensity (1–3 cm/year) in the northern (25° S–15° S) and southern parts (40° S–30° S) of the domain. However, while summer presents null to positive values in the central part of the domain (35° S–25° S), winter presents negative trends at these latitudes (Fig. 5b, c, f, g).

The spatial trends in the summer also present significant changes in the mean wave direction, particularly to the east of 45° W. Coastal regions from 25° S to 10° S, where waves from the east quadrant dominate (Fig. 3d), present a clockwise shift in the mean wave direction between 1 and 2°/year. For instance, this shift is enough to change the dominant quadrant from east to south in 42 years, which potentially increases wave damage on the southern shoreline of the state of Rio de Janeiro ($\sim 23°$ S). This region also presents an increase in the lifetime of these events (between 0.15 and 0.20 h per year; Fig. 5).

In the winter, the central portion of the study domain (30° S–25° S) presents significant negative trends in the mean intensity (~ -2 cm/year), lifetime (~ -0.1 h/year), and mean wave direction of the events (~ -2 °/year). These changes mainly affect the coast of the states of Santa Catarina and Paraná (the shoreline between 30° S and 25° S), and the offshore region is known as Santos Basin, in which a high concentration of oil platforms are installed.

The anti-clockwise shift may result in more extreme waves approaching the coast from the southeast and creating the northwards alongshore transport that, together with the major reduction in the winter event intensity, might affect sediment transport in the region.

3.4 Directional changes in the wave power

The small number of events (≤ 2.5 events per grid per season) does not allow for a reliable assessment of the spatial mean wave direction and peak period trends. To overcome this limitation, the trends in these wave parameters were analysed at points that represent strategic regions of changes according to the previous analysis: three points that represent the regions offshore the northern (20.0° S), central (25.3° S), and southern (31.5° S) coast of the domain (Fig. 1) These points were determined based on buoy locations, thus allowing the evaluation of ERA5 against in situ data (see Suppl. Text 1). The directional density distribution of the peak period and wave power are used to better view the joint impact of changes in the mean wave direction, wave period, and, indirectly, Hs offshore of the Brazilian coast.

In general, we find significant changes in the directional distribution of the wave power (Fig. 6) and peak period (Fig. 7) at all stations. Some locations also present increasing wave power, observed by the radial shift away from the centre of the polar plot. This increase is mainly associated with Hs changes (wave power $\propto Hs^2$). However, in some locations, it is also related to the rising wave period (Fig. 7).
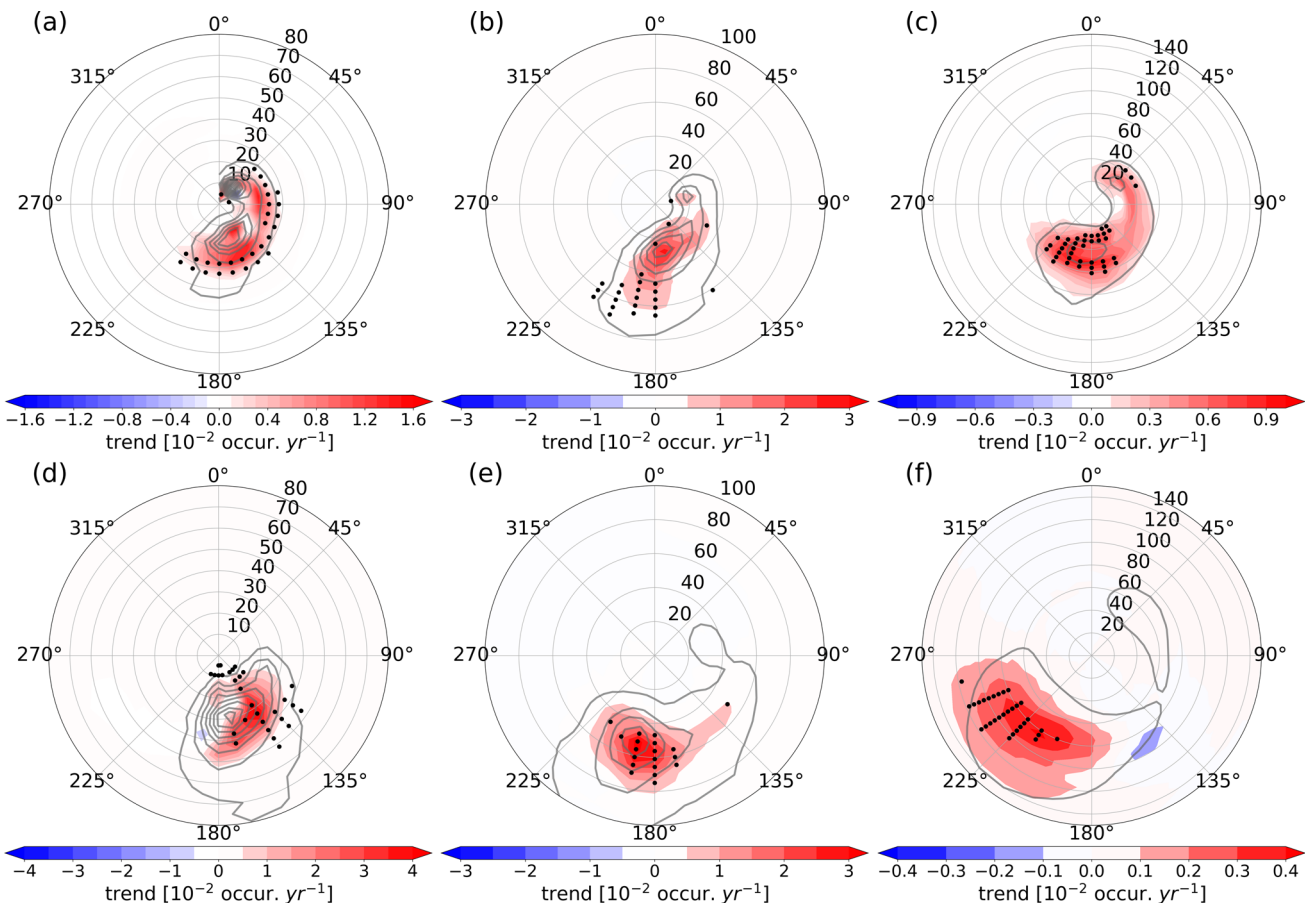
Fig. 6 Trends in the directional distribution of the wave power associated with extreme events computed for ERA5 at the **a** and **b** Vitória (20.0° S; 39.7° W), **b** and **e** Santos (25.3° S; 44.9° W), and **c** and **f** Rio Grande (31.5° S; 49.9° W) points. The trends were computed using the ERA5 products for the **a–c** summer (DJF) and **d–f** winter (JJA). The angles on the polar plot represent the mean wave direction (from), where 0° and 90° represent the North and East, respectively. The radial axis represents wave power ($kWm^{-3}s^{-1}$), and the shaded colour represents the trend of occurrence per year (scaled by 10^2). The grey line contours indicate mean occurrence distribution computed for the ERA5 climatology (average over the 1979–2020 period), contoured each 0.2 occurrence interval starting from 0.1. The occurrence is obtained by the density multiplied by the number of samples. The black dots indicate trends with p-value ≤ 0.05 (Mann-Kendall)

In the summer, the VT Station presents an increase in extreme event occurrence from the east, i.e., perpendicular to the shoreline, with a wave power of $\sim 20\,kWm^{-3}s^{-1}$, followed by an increase in the peak period (10–12.5 s). In the winter, this location presents a slight increase in the wave power (40 $kWm^{-3}s^{-1}$) and peak period (15 s) of southeasterly waves, which indicates a counterclock shift of the dominant wave direction in the season.

At the Santos Station (ST, 25.3° S), the wave power from the southern quadrant is still dominant. However, there is a trend of increase of events with approximately 60 $kWm^{-3}s^{-1}$ in summer, while there is a more directional spreaded trend in winter (between 120 and 225°). Despite the spread in density, the winter trends show higher values of wave power from the south and smaller values from the southwest (225°) and southeast (135°), which can be directly connected with the increase in the wave period from the south

(15 s), indicating more swell propagating from this direction. On the other hand, there is an increase in the southeasterly wave occurrence with the higher peak period (12.5–15 s). Both wave systems influence the northern coast of the state of São Paulo and the southern coast of Rio de Janeiro, acting almost perpendicular to the shoreline.

The Rio Grande Station (RG, 31.5° S) represents the southern portion of the study domain, where the wave power is higher compared to the stations to its north (40 and 80 $kWm^{-3}s^{-1}$). The RG Station presents small but significant changes in the maximum density core of the wave power directional distribution in both seasons. In the summer, the wave power distribution trends follow similar directional distribution as the climatology, only showing an increase in the occurrence of events from the north quadrant. The peak period trends present an increase in the south-southwestern sector, indicating that this trend is driven by swell propaga-
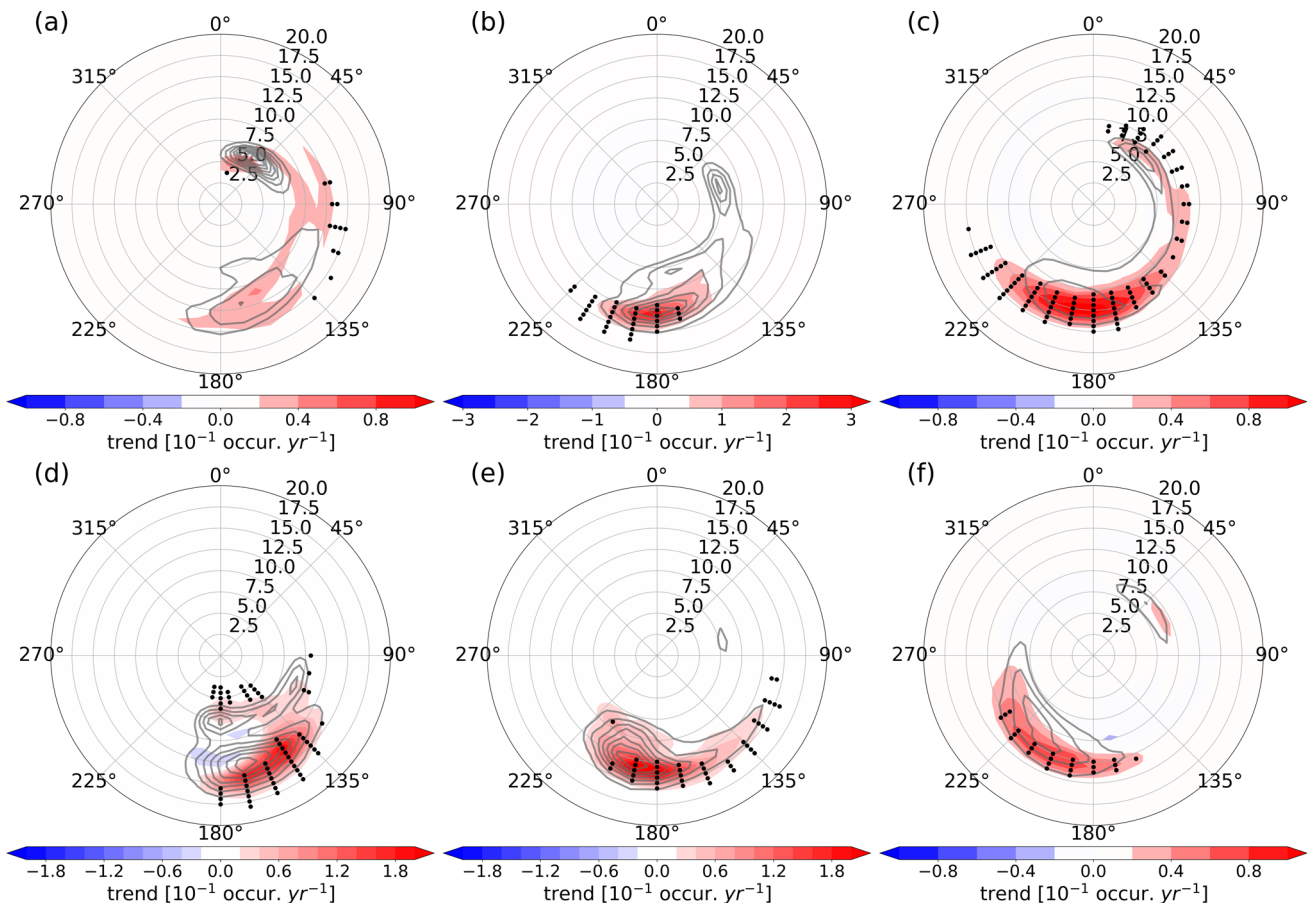
Fig. 7 Trends in the directional distribution of the peak period associated with extreme events computed for ERA5 at the **a** and **d** Vitória (20.0° S; 39.7° W), **b** and **e** Santos (25.3° S; 44.9° W), and **c** and **f** Rio Grande (31.5° S; 49.9° W) points. The trends were computed using the ERA5 products for the **a–c** summer (DJF) and **d–f** winter (JJA). The angles on the polar plot represent the mean wave direction (from), where 0° and 90° represent the North and East, respectively. The radial axis represents the peak period (s^{-1}), and the shaded colour represents the trend of occurrence per year (scaled by 10^1). The grey line contours indicate mean occurrence distribution computed for the ERA5 climatology (average over the 1979–2020 period), contoured each 2 occurrence interval starting from 2. The occurrence is obtained by the density multiplied by the number of samples. The black dots indicate trends with p-value ≤ 0.05 (Mann-Kendall)

tion (peak period of approximately 12.5–15 s). Moreover, the RG Station also experiences an increased occurrence of east-northeasterly extreme wave events with a lower peak period (7.5 s) in the summer. In the winter, in turn, the RG Station presents a clockwise shift in the occurrence of extreme events with a wave power of approximately $100\,kWm^{-3}s^{-1}$, which is related to an increase in the peak period from the wave propagating from south-southwest (180–240°), parallel to the main shoreline.

4 Discussion

The findings in this study show overall changes in the extreme wave events in terms of their lifetime, intensity, direction, peak period, and wave power. The trends differ in the summer and winter due to differences in the dominant atmospheric

setup in each season. The changes are also distinct among the study region's northern, central, and southern portions due to its exposure to different atmospheric systems. The discussion focuses on areas with significant changes, linking them with the potential impact on the coast. We also discuss the mechanisms driving these changes.

4.1 General trends of extreme wave events

The spatial distribution of the 95th-percentile Hs reveals positive trends in most of the study domain, with statistically significant changes observed mainly in the northern and southwestern portions. Evidence of increased extreme wave percentiles in the northern and southern parts of the domain is supported by satellite spatial trends, both for the significant wave height and surface winds (Suppl. Text 2 and Young and Ribal, 2019).
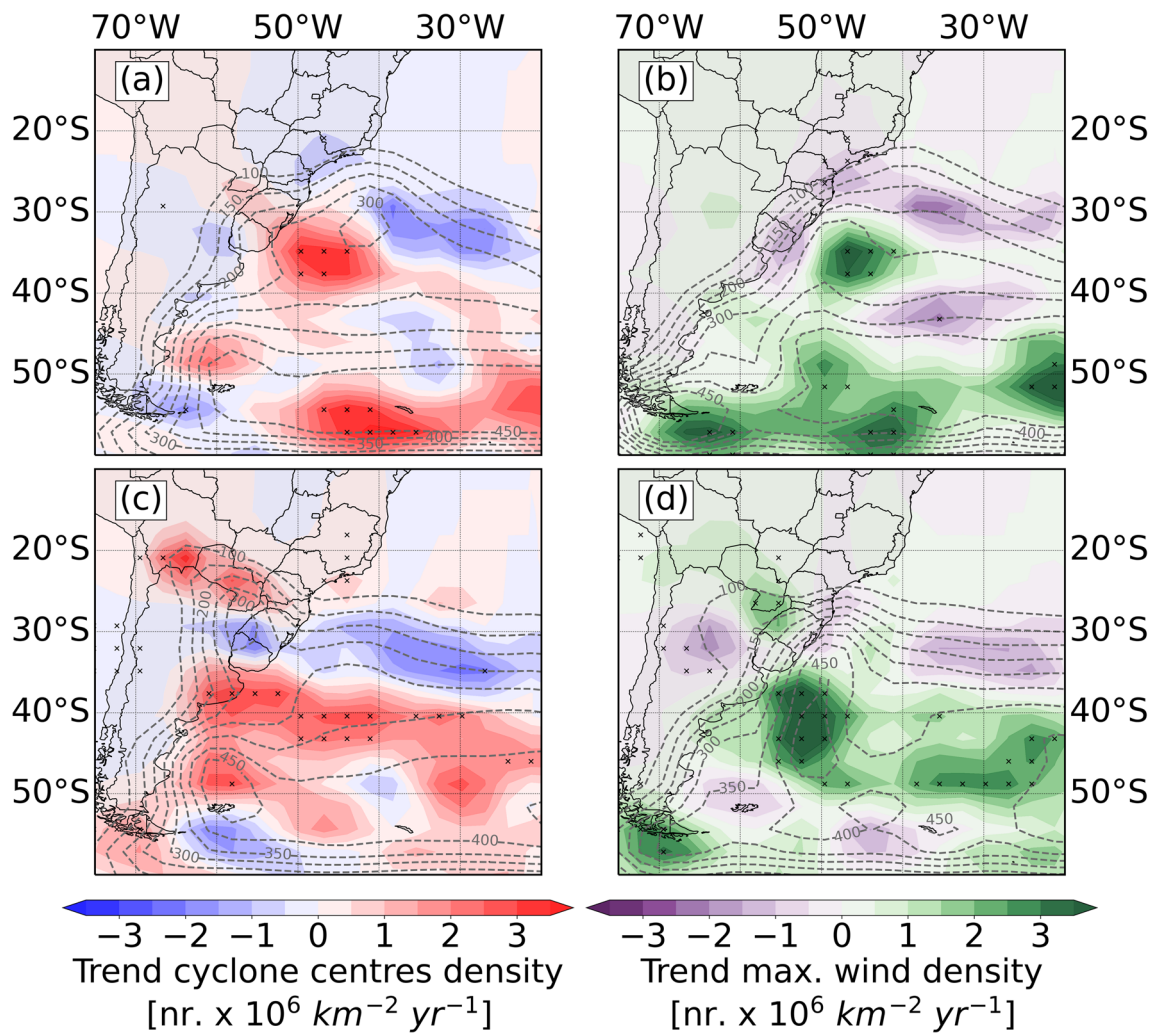
Fig. 8 Trends in the density (number x 10^{-6} km^{-2} $year^{-1}$) of **a** and **c** cyclone centres (minimum vorticity at 850 hPa) and **b** and **d** location of the maximum wind speed at 10 m associated with cyclones for the **a** and **b** summer (DJF) and **c** and **d** winter (JJA). The contour lines indicate the ERA5 climatology (mean values over the 1979–2020 period). Trends with p-value ≤ 0.05 are presented with black crosses (Mann-Kendall)

Our results show that in the SWSA, summertime extreme wave events are becoming more intense and longer-lived. These findings answer the questions raised in previous research (Gramcianinov et al. 2022), in which an increase in summertime local extreme wave occurrences was found but could not be easily explained (i.e., whether it was related to changes in the lifetime and/or the frequency of the events). Through the analysis performed herein, we find that the increased frequency reported by these authors was due to the increase in event numbers and the high event lifetime. The winter presents negative to null trend values in the central portion of the domain. The heterogeneous spatial distributions of these trend patterns may be why the winter time series do not present significant trends.

The mean wave direction of the events in the summer shifts clockwise northwards of 25.5° S, which has a prevalence of

east-southeasterly waves. The directional wave power analysis at 25.3° S reveals a counterclockwise shift of the wave power maximum occurrence further south. These findings agree with previous research (Odériz et al. 2021), in which the dominant southeasterly wave system was found to shift clockwise in the subtropics while the dominant southerly wave system shifted counterclockwise in the extratropics. In the winter, when the southern wave quadrant dominates the study domain, the general shift is counterclockwise. However, there is an increase in the westerly wave system in the extratropics, which justifies the widespread wave power flux changes at the ST (25.3°S) and RG (31.5° S) Stations from southwest to southeast.

4.2 Coastal exposure to wave events changes

In summer, the region between 23° S and 15° S experiences an increased frequency and lifetime of these events, followed by a clockwise shift in the mean wave direction. In an area dominated by east-southeasterly extreme waves, this shift results in more extreme events from the south-southeast, which is related to episodes of erosion in this region (Muehe 2018). Nevertheless, the directional wave flux analysis at 20° S shows that the wave systems from the south-southwest do not present a significant increase in the wave power or peak period. Instead, easterly waves with a moderate wave power (20 $kWm^{-3}s^{-1}$) and wave period (10 s) increase. These waves propagate towards the approximately S-N-oriented coast of the state of Espírito Santo ($\sim$ 20° S) and are also associated with higher lifetime events. More than 15% of this segment of the Brazilian coast is facing erosion, even with its high diversity of coastal environments (Muehe 2018). Although most erosive events in this region are associated with SE swells, the increase in medium-energy events may lead to morphological responses equivalent to those of high-energy events (Ferreira 2005).

The increased occurrence of extreme events from the south-southeast may also affect the W-E-oriented coast of northern São Paulo and Rio de Janeiro ($\sim$ 23°S). The reported increase in the lifetime of the events in the summer intensifies the exposure of this shoreline segment. The directional wave flux analysis at the station located offshore of this coastal region (ST, 25.3°S) confirms this vulnerability, showing an increase in southerly waves with large wave power (between 40 and 60 $kWm^{-3}s^{-1}$), followed by a rise in the wave peak period from the same quadrant. In the winter, the high energetic waves spread from south-southwestern to south-southeast, which increases the exposure angle of the coast and affects the cross-shore and longshore sediment transport (Harley et al. 2017; Carvalho et al. 2021). The last Brazilian coastal erosion report presented that 4% and 12% of the São Paulo and Rio de Janeiro coasts are being eroded, respectively. However, 12% and 38% of these same coastal segments tend to erosion, meaning that they present erosion signals without significant changes in the mean shoreline. Specifically, the northern portion of São Paulo shows some municipalities reaching erosion rates between 1.17 and 1.9 m/year since the 1960s (Souza and Luna 2009).

The relationship between the changes in the extreme wave event characteristics in the study domain and the increase in erosion is complex, as shoreline changes depend on several other factions in addition to the wave climate. Inappropriate coastal development and the consequential non-natural changes in the sediment balance (i.e., destruction of dunes and mangroves) are the top erosion drivers (e.g., Muehe 2018; Mentaschi et al. 2018). Nevertheless, they can be accelerated by wave event modification. Minor variations in the wave direction can change sediment transport by varying the cross-shore and alongshore circulation. The influence of the wave changes will thus depend on the coastline orientation and morphology.

4.3 Possible driven mechanisms of wave climate changes

The general increase in the southerly wave power and wave period reported in the present study can be associated with the polewards shift of the South Atlantic storm track and the increase in Southern Ocean-generated waves (e.g., Caires and Sterl 2005). However, as previously discussed (Hemer et al. 2010), the changes and variabilities in South Atlantic wave directions are not directly associated with Southern Ocean changes.

The extreme wave changes observed in summer agree with past studies that reported a weakening in the SASH equatorial flank (Zilli et al. 2019; Reboita et al. 2019) and the SACZ polewards migration as a consequence of the southwestwards shift of the SASH, both of which are related to the expansion of the Hadley cell (Lu et al. 2008; Nguyen et al. 2015). These shifts can be directly associated with the higher frequency of events with moderate wave power ($\sim$ 20 $kWm^{-3}s^{-1}$) from the east at 20° S and the increased intensity and lifetime of the events along the region off the coast between 20° S and 15° S. The Hadley cell expansion also affects the upper-level jet position and, consequently, the storm track. Therefore, a general southwards shift of the storm track has been observed, including in its subtropical branch. de Jesus et al. (2020) showed a cyclone track decrease along the southeastern Brazilian coast (25° S–35° S) and an increase at approximately 38° S, between Uruguay and Argentina. Between 1979 and 2020, changes in the extratropical cyclone position presented a south-westwards shift of the higher-density core in the summer (Fig. 8a) in agreement with the previous findings. The higher density of cyclone centres between 40° S and 30° S is associated with their slow displacement in the summer and their role in establishing the SACZ. The persistence of the maximum winds associated with these cyclones follows this shift (Fig. 8b), which supports the wave power and peak period increase from the south-southwest at 25° S and 31.5° S. Another important aspect is that extratropical cyclones generated at approximately 35° S are usually more intense due to the influence of the Andes Cordillera and high sea surface temperature gradients (Gramcianinov et al. 2019). Thus, the systems originating at that location are commonly related to the generation of extreme waves in the domain (Gramcianinov et al. 2022). The activity of stronger extratropical cyclones agrees with the increase in the intensity and lifetime of the wave events in the southern portion of the domain (40° S–30° S) and the W-E oriented coast at approximately 23° S.

Changes in the winter also follow the southwards shift of the storm track (Fig. 8c), which is shown by the decrease in the cyclone centres between 27° S and 35° S and the increase between 35° S and 40° S. With more cyclones developing near the coast at approximately 35° S and eastwards displacement, the increase in the directional spread between south-southwest is expected. The maximum wind associated with the cyclones shifts towards the coast (Fig. 8d), allowing the development of a south-southwesterly fetch along the shoreline. This local forcing is reflected in the smaller periods from the southwesterly waves in the southern portion of the domain (31.5° S). Following the summer discussion, the southwards shift of the storm track results in a higher peak period and wave power from the wave systems from the south, as also reported by Lobeto et al. (2021). However, winter differs from summer, as it presents an increase in the influence of waves from the southwest to the southeast.

5 Conclusion

Both the traditional percentile- and event-based wave methods reveal significant changes in the extreme wave climate in some locations of the southwestern South Atlantic. Summer and winter present statistically significant spatial changes in the lifetimes, intensities, and mean directions of events. In this study, we show that extreme events are being modified by storm track changes, potentially as a consequence of the Hadley cell expansion, as discussed in previous work. The result of this shift is experienced differently in summer and winter northwards of 23° due to the action of the SASH in the former. Under the influence of a southwestwards-shifted SASH, there is an increase in the easterly moderate wave power events towards the coast segment at this latitude. In the rest of the domain, longer period waves increase the southerly wave power, with an increase in the directional spread of the events from SW to SE due to the shift of the extratropical cyclones fetches southwestwards.

Studying extreme wave climate conditions and storms in the SWSA is critical and highly relevant for engineering practices. Extreme waves are responsible for coastal flooding and affect coastal erosion (e.g., Machado and Calliari 2016; Parise et al. 2009; Harley et al. 2017). Understanding these processes is crucial for the design, maintenance, and safety of ship vessels and offshore and coastal structures (e.g., Bitner-Gregersen et al. 2018; Vettor and Guedes Soares 2020). Both climate natural variability and human-induced shifts can result in long-term changes in the extreme wave climate in the SWSA (Silva et al. 2020; Gramcianinov et al. 2022), which may require adaptation measures. Thus, the outcomes of this work are relevant to the region since the variety of shoreline orientations makes the Brazilian coast susceptible to even small changes in the wave event characteristics.

The estimated changes in the SWSA storm regime derived in the present study are a valuable factor in identifying areas that are most vulnerable to climate change hazards and are a valuable tool for engineers and stakeholders working towards the sustainable development of maritime activities. Despite the dataset limitation, our results agree with the large-scale atmospheric changes reported by previous studies. They can be used as a reference considering the consequences of the Hadley cell expansion, which is widely reported under current climate conditions and future climate projections. Future analyses should investigate more extended datasets and climate simulations to better understand the roles of natural variability and climate change in the trends reported herein.

project maintained by the Brazilian Navy as part of the Brazilian Global Ocean Observation System (GOOS-Brasil) (available on https://www. marinha.mil.br/chm/dados-do-goos-brasil/pnboia-mapa, last access: 10 May 2022). The cyclone tracks used in this study were obtained from the "Alantic extratropical cyclone tracks in 41 years of ERA5 and CFSR/CFSv2 databases" (https://doi.org/10.17632/kwcvfr52hp.4).

Code Availability The codes are available under request by email to the corresponding author.

Declarations

Ethics approval Not applicable

Consent to participate Not applicable

Consent for publication Not applicable

Conflict of interest The authors declare no competing interests.

References

Amante C, Eakins B (2009) ETOPO1 1 Arc-minute global relief model: procedures, data sources and analysis. NOAA technical memorandum NESDIS NGDC-24. National geophysical data center, NOAA. https://doi.org/10.7289/V5C8276M

ANTAQ (2022) Anuário da Agência Nacional de Transporttes Aquaviários (ANTAQ). Annual report of the national water transportation agency, Brazil (in Portuguese), https://anuario.antaq.gov.br, [last access: 12 May 2022]

Ardhuin F, Rogers E, Babanin AV et al (2010) Semiempirical dissipation source functions for ocean waves part I: definition, calibration, and validation. J Phys Oceanogr 40(9):1917–1941. https://doi.org/10.1175/2010jpo4324.1

Belmonte Rivas M, Stoffelen A (2019) Characterizing ERA-interim and ERA 5 surface wind biases using ASCAT. Ocean Sci 15(3):831–852. https://doi.org/10.5194/os-15-831-2019

Bitner-Gregersen EM, Vanem E, Gramstad O et al (2018) Climate change and safe design of ship structures. Ocean Eng 149:226–237. https://doi.org/10.1016/j.oceaneng.2017.12.023

C3S (2017) ERA5: fifth generation of ECMWF atmospheric reanalyses of the global climate. Copernicus climate change service (C3S) climate data store (CDS), https://cds.climate.copernicus.eu, Access 20 Jan 2021

Caires S, Sterl A (2005) 100-year return value estimates for ocean wind speed and significant wave height from the ERA-40 data. J Clim 18(7):1032–1048. https://doi.org/10.1175/JCLI-3312.1

Campos RM, Alves JHGM, Guedes Soares C et al (2018) Extreme wind-wave modeling and analysis in the South Atlantic ocean. Ocean Model 124:75–93. https://doi.org/10.1016/j.ocemod.2018.02.002

Campos R, Soares CG, Alves JHGM et al (2019) Regional long-term extreme wave analysis using hindcast data from the South Atlantic Ocean. Ocean Eng 179:202–212. https://doi.org/10.1016/j.oceaneng.2019.03.023

Campos RM, Gramcianinov CB, de Camargo R et al (2022) Assessment and calibration of ERA 5 severe winds in the Atlantic Ocean using satellite data. Remote Sens 14(19):4918. https://doi.org/10.3390/rs14194918

Carvalho BC, de Barros FML, da Silva PL, et al (2021) Morphological variability of sandy beaches due to variable oceanographic conditions: a study case of oceanic beaches of Rio de Janeiro city (Brazil). J Coast Conserv 25(2). https://doi.org/10.1007/s11852-021-00821-8

Casas-Prat M, Wang XL, Mori N et al (2022) Effects of internal climate variability on historical ocean wave height trend assessment. Frontiers Mar Sci 9. https://doi.org/10.3389/fmars.2022.847017

Cornett AM (2008) A global wave energy resource assessment. In: Proceedings of the eighteenth international offshore and polar conference, Vancouver, Canada, July, 2008, pp ISOPE–2008–TPC–579

da Rocha RP, Sugahara S, da Silveira RB (2004) sea waves generated by extratropical cyclones in the South Atlantic Ocean: hindcast and validation against altimeter data. Weather Forecast 19(2):398–410. https://doi.org/10.1175/1520-0434(2004)019<0398:swgbec>2.0.co;2

Dalagnol R, Gramcianinov CB, Crespo NM et al (2022) Extreme rainfall and its impacts in the Brazilian Minas Gerais state in January 2020: can we blame climate change? Climate Resilience and Sustainability 1(1):1–15. https://doi.org/10.1002/cli2.15

de Jesus EM, da Rocha RP, Crespo NM et al (2020) Multi-model climate projections of the main cyclogenesis hot-spots and associated winds over the eastern coast of South America. Climate Dynamics 56(1–2):537–557. https://doi.org/10.1007/s00382-020-05490-1

Dobrynin M, Murawsky J, Yang S (2012) Evolution of the global wind wave climate in CMIP5 experiments. Geophys Res Lett 39(17):2–7. https://doi.org/10.1029/2012GL052843

Dragani WC, Cerne BS, Campetella CM et al (2013) Synoptic patterns associated with the highest wind-waves at the mouth of the Río de la Plata Estuary. Dynamics of Atmospheres and Oceans 61–62:1–13. https://doi.org/10.1016/j.dynatmoce.2013.02.001

Ferreira O (2005) Storm groups versus extreme single storms: predicted erosion and management consequences. Journal of coastal research pp 221–227. https://www.jstor.org/stable/25736987

Goda Y (2010) Random seas and design of maritime structures. World Scientific. https://doi.org/10.1142/7425

Gramcianinov CB, Campos RM, de Camargo R, et al. (2020) Atlantic extratropical cyclone tracks in 41 years of ERA5 and CFSR/CFSv2 databases. Mendeley Data V4. https://doi.org/10.17632/kwcvfr52hp.4

Gramcianinov CB, Campos RM, Guedes Soares C et al (2020) Extreme waves generated by cyclonic winds in the western portion of the South Atlantic Ocean. Ocean Eng 213(1):107,745. https://doi.org/10.1016/j.oceaneng.2020.107745

Gramcianinov CB, Hodges KI, de Camargo R (2019) The properties and genesis environments of South Atlantic cyclones. Clim Dyn 53(7–8):4115–4140. https://doi.org/10.1007/s00382-019-04778-1

Gramcianinov CB, Campos RM, de Camargo R et al (2020) Analysis of Atlantic extratropical storm tracks characteristics in 41 years of ERA5 and CFSR/CFSv2 databases. Ocean Eng 216(108):111. https://doi.org/10.1016/j.oceaneng.2020.108111

Gramcianinov CB, de Camargo R, Campos RM et al (2022) Impact of extratropical cyclone intensity and speed on the extreme wave trends in the Atlantic Ocean. Climate Dynamics. https://doi.org/10.1007/s00382-022-06390-2

Guillou N (2020) Estimating wave energy flux from significant wave height and peak period. Renew Energy 155:1383–1393. https://doi.org/10.1016/j.renene.2020.03.124

Hamilton SE, Casey D (2016) Creation of a high spatio-temporal resolution global database of continuous mangrove forest cover for the 21st century (CGMFC-21). Glob Ecol Biogeogr 25(6):729–738. https://doi.org/10.1111/geb.12449

Harley MD, Turner IL, Kinsela MA, et al (2017) Extreme coastal erosion enhanced by anomalous extratropical storm wave direction. Scientific Reports 7(1). https://doi.org/10.1038/s41598-017-05792-1

Hemer MA, Church JA, Hunter JR (2010) Variability and trends in the directional wave climate of the Southern Hemisphere. Int J Climatol 30(4):475–491. https://doi.org/10.1002/joc.1900

Hersbach H, Bell B, Berrisford P et al (2020) The ERA 5 global reanalysis. Q J R Meteorol Soc 146(730):1999–2049. https://doi.org/10.1002/qj.3803

Hodges KI (1994) A general method for tracking analysis and its application to meteorological data. Mon Weather Rev 122(11):2573–2586. https://doi.org/10.1175/1520-0493(1994)122<2573:AGMFTA>2.0.CO;2

Hodges KI (1995) Feature tracking on the unit sphere. Mon Weather Rev 123(12):3458–3465. https://doi.org/10.1175/1520-0493(1995)123<3458:FTOTUS>2.0.CO;2

Hodges KI (1996) Spherical nonparametric estimators applied to the UGAMP model integration for AMIP. Mon Weather Rev 124(12):2914–2932. https://doi.org/10.1175/1520-0493(1996)124<2914:SNEATT>2.0.CO;2

Hodges KI, Lee RW, Bengtsson L (2011) A comparison of extratropical cyclones in recent reanalyses ERA-Interim, NASA MERRA, NCEP CFSR, and JRA-25. J Clim 24(18):4888–4906. https://doi.org/10.1175/2011JCLI4097.1

Hoskins BJ, Hodges KI (2002) New perspectives on the Northern hemisphere winter storm tracks. J Atmos Sci 59(6):1041–1061. https://doi.org/10.1175/1520-0469(2002)059<1041:NPOTNH>2.0.CO;2

Hoskins BJ, Hodges KI (2005) A new perspective on Southern hemisphere storm tracks. J Clim 18(20):4108–4129. https://doi.org/10.1175/JCLI3570.1

ICMBio (2018) Atlas dos Manguezais do Brasil (Brazilian Mangrove Atlas) [in Portuguese]. Instituto Chico Mendes de Conservação da Biodiversidade (ICMBio), Ministério do Meio Ambiente - MMA (Ministry of the Environment), Brazil

Kendall M (1975) Rank correlation methods, 4th edn. Charles Griffin, London

Kodama Y (1992) Large-scale common features of subtropical precipitation zones (the Baiu Frontal Zone, the SPCZ, and the SACZ) Part I: characteristics of subtropical frontal zones. J Meteorol Soc Jpn Ser II 70(4):813–836. https://doi.org/10.2151/jmsj1965.70.4_813

Law-Chune S, Aouf L, Dalphinet A et al (2021) WAVERYS: a CMEMS global wave reanalysis during the altimetry period. Ocean Dynamics 71(3):357–378. https://doi.org/10.1007/s10236-020-01433-w

Lemos G, Semedo A, Dobrynin M et al (2019) Mid-twenty-first century global wave climate projections: results from a dynamic CMIP 5 based ensemble. Glob Planet Chang 172:69–87. https://doi.org/10.1016/j.gloplacha.2018.09.011

Leo FD, Solari S, Besio G (2020) Extreme wave analysis based on atmospheric pattern classification: an application along the Italian coast. Nat Hazards Earth Syst Sci 20(5):1233–1246. https://doi.org/10.5194/nhess-20-1233-2020

Liu Q, Rogers WE, Babanin AV et al (2019) Observation-based source terms in the third-generation wave model WAVEWATCH III: updates and verification. J Phys Oceanogr 49(2):489–517. https://doi.org/10.1175/JPO-D-18-0137.1

Liu Q, Babanin A (2021) Product user guide for the WW3-ST6 global wave hindcasts. https://doi.org/10.5281/zenodo.4497717

Liu Q, Babanin AV, Rogers WE, et al (2021) Global wave hindcasts using the observation-based source terms: description and validation. J Adv Model Earth Syst 13(8). https://doi.org/10.1029/2021MS002493

Lobeto H, Menendez M, Losada IJ (2021) Projections of directional spectra help to unravel the future behavior of wind waves. Frontiers Marine Sci 8(May). https://doi.org/10.3389/fmars.2021.655490

Lu J, Chen G, Frierson DMW (2008) Response of the zonal mean atmospheric circulation to El Niño versus global warming. J Clim 21(22):5835–5851. https://doi.org/10.1175/2008jcli2200.1

Machado AA, Calliari LJ, Melo E et al (2010) Historical assessment of extreme coastal sea state conditions in southern Brazil and their relation to erosion episodes. Pan-Amer J Aquatic Sci 5(2):105–114 (https://panamjas.org/pdf_artigos/PANAMJAS_5(2)_277-286.pdf)

Machado AA, Calliari LJ (2016) Synoptic systems generators of extreme wind in Southern Brazil: atmospheric conditions and consequences in the coastal zone. J Coast Res 1(75):1182–1186. https://doi.org/10.2112/SI75-237.1

Mann HB (1945) Nonparametric tests against trend. Econometrica 13(3):245–259 (http://www.jstor.org/stable/1907187)

Marcello F, Wainer I, Rodrigues RR (2018) South Atlantic subtropical gyre late twentieth century changes. J Geophys Res: Oceans 123(8):5194–5209. https://doi.org/10.1029/2018jc013815

Mentaschi L, Vousdoukas MI, Pekel JF, et al (2018) Global long-term observations of coastal erosion and accretion. Scientific Reports 8(1). https://doi.org/10.1038/s41598-018-30904-w

Meucci A, Young IR, Hemer M et al (2020) Projected 21st century changes in extreme wind-wave events. Sci Adv 6(24):eaaz7295. https://doi.org/10.1126/sciadv.aaz7295

Muehe D (2018) Panorama da Erosão Costeira no Brasil (Overview of Coastal Erosion in Brazil) [in Portuguese]. Ministério do Meio Ambiente - MMA (Ministry of the Environment), Brazil

Nguyen H, Lucas C, Evans A et al (2015) Expansion of the southern hemisphere Hadley cell in response to greenhouse gas forcing. J Clim 28(20):8067–8077. https://doi.org/10.1175/jcli-d-15-0139.1

Odériz I, Silva R, Mortlock TR et al (2021) Natural variability and warming signals in global ocean wave climates. Geophys Res Lett 48(11):1–12. https://doi.org/10.1029/2021GL093622

Parise CK, Calliari LJ, Krusche N (2009) Extreme storm surges in the south of Brazil: atmospheric conditions and shore erosion. Braz J Oceanogr 57:175–188

Pereira-Filho GH, Mendes VR, Perry CT et al (2021) Growing at the limit: reef growth sensitivity to climate and oceanographic changes in the South Western Atlantic. Glob Planet Chang 201(103):479. https://doi.org/10.1016/j.gloplacha.2021.103479

Pezzi LP, Quadro MFL, Lorenzzetti JA et al (2022) The effect of oceanic South Atlantic convergence zone episodes on regional SST anomalies: the roles of heat fluxes and upper-ocean dynamics. Climate Dynamics. https://doi.org/10.1007/s00382-022-06195-3

Rascle N, Ardhuin F (2013) A global wave parameter database for geophysical applications. Part 2: Model validation with improved source term parameterization. Ocean Model 70:174–188. https://doi.org/10.1016/j.ocemod.2012.12.001

Reboita MS, da Rocha RP, Ambrizzi T et al (2010) South Atlantic Ocean cyclogenesis climatology simulated by regional climate model (RegCM3). Climate Dynamics 35(7):1331–1347. https://doi.org/10.1007/s00382-009-0668-7

Reboita MS, Ambrizzi T, Silva BA et al (2019) The South Atlantic subtropical anticyclone: present and future climate. Frontiers

in Earth Science 7(February):1–15. https://doi.org/10.3389/feart.2019.00008

Reguero BG, Losada IJ, Méndez FJ (2019) A recent increase in global wave power as a consequence of oceanic warming. Nature Communications 10(205):1–14. https://doi.org/10.1038/s41467-018-08066-0

Rodrigues RR, Taschetto AS, Sen Gupta A et al (2019) Common cause for severe droughts in South America and marine heatwaves in the South Atlantic. Nat Geosci 12(8):620–626. https://doi.org/10.1038/s41561-019-0393-8

Saha S, Moorthi S, Pan HL et al (2010) The NCEP climate forecast system reanalysis. Bull Am Meteorol Soc 91(8):1015–1058. https://doi.org/10.1175/2010bams3001.1

Sen PK (1968) Estimates of the regression coefficient based on kendall's tau. J Am Stat Assoc 63(324):1379–1389. https://doi.org/10.1080/01621459.1968.10480934

Sharmar VD, Markina MY, Gulev SK (2021) Global ocean wind-wave model hindcasts forced by different reanalyzes: a comparative assessment. J Geophys Res: Oceans 126(1):1–19. https://doi.org/10.1029/2020JC016710

Silva AP, Klein AH, Fetter-Filho AF et al (2020) Climate-induced variability in South Atlantic wave direction over the past three millennia. Scientific Reports 10(1):1–12. https://doi.org/10.1038/s41598-020-75265-5

Souza CRdG, Luna GdC (2009) Taxas de retrogradação e balanço sedimentar em praias sob risco muito alto de erosão no município de Ubatuba (Litoral Norte de São Paulo). Quaternary and Environmental Geosciences 1(1). https://doi.org/10.5380/abequa.v1i1.14489

Souza CRdG, Souza AP, Harari J (2019) Long term analysis of meteorological-oceanographic extreme events for the baixada santista region. In: Climate change in Santos Brazil: projections, impacts and adaptation options. Springer International Publishing, pp 97–134, https://doi.org/10.1007/978-3-319-96535-2_6

Takbash A, Young IR (2020) Long-term and seasonal trends in global wave height extremes derived from ERA-5 reanalysis data. J Marine Sci Eng 8(12):1–16. https://doi.org/10.3390/jmse8121015

UN (1982) The Law of the Sea. Convention on the Law of the Sea, Dec 10, 1982, 1833 UNTS 397, http://treaties.un.org/doc/Publication/UNTS/Volume%201833/volume-1833-A-31363-English.pdf

Vettor R, Guedes Soares C (2020) A global view on bimodal wave spectra and crossing seas from ERA-Interim. Ocean Eng 210(107):439. https://doi.org/10.1016/j.oceaneng.2020.107439

Wang F, Shao W, Yu H et al (2020) Re-evaluation of the power of the Mann-Kendall test for detecting monotonic trends in hydrometeorological time series. Frontiers Earth Sci 8. https://doi.org/10.3389/feart.2020.00014 www.frontiersin.org/articles/10.3389/feart.2020.00014

Weisse R, Günther H (2007) Wave climate and long-term changes for the Southern North Sea obtained from a high-resolution hindcast 1958–2002. Ocean Dynamics 57(3):161–172. https://doi.org/10.1007/s10236-006-0094-x

Wu S, Liu C, Chen X (2015) Offshore wave energy resource assessment in the east china sea. Renewable Energy 76:628–636. https://doi.org/10.1016/j.renene.2014.11.054

WW3 Development Group (2019) User manual and system documentation of WAVEWATCH III® version 6.07. WAVEWATCH III Development Group, NOAA/NWS/NCEP/MMAB College Park, MD, USA

Young IR, Ribal A (2019) Multiplatform evaluation of global trends in wind speed and wave height. Science 364(6440):548–552. https://doi.org/10.1126/science.aav9527

Zamboni A, Nicolodi JL (2008) Macrodiagnóstico da Zona Costeira e Marinha do Brasil (Macrodiagnosis of the Brazilian Coastal and Marine Zone) [in Portuguese]. Ministério do Meio Ambiente - MMA (Ministry of the Environment), Brazil

Zilli MT, Carvalho LM, Lintner BR (2019) The poleward shift of South Atlantic convergence zone in recent decades. Climate Dynamics 52(5–6):2545–2563. https://doi.org/10.1007/s00382-018-4277-1

Publisher's Note Springer Nature remains neutral with regard to jurisdictional claims in published maps and institutional affiliations.